# Mono- and Bicyclic Analogs of Parathyroid Hormone-Related Protein. 2. Conformational Analysis of Antagonists by CD, NMR, and Distance Geometry Calculations†

Stefano Maretto,‡,§ Stefano Mammi,‡ Elisa Bissacco,‡ Evaristo Peggion,‡ Alessandro Bisello,|| Michael Rosenblatt,|| Michael Chorev,|| and Dale F. Mierke*,§,⊥

*Department of Organic Chemistry, University of Padova, Biopolymer Research Center, Via Marzolo 1, I-35131 Padova, Italy, Gustaf H. Carlson School of Chemistry, Clark University, 950 Main Street, Worcester, Massachusetts 01610, Division of Bone and Mineral Metabolism, Harvard−Thorndike and Charles A. Dana Laboratories, Beth Israel Deconess Medical Center, 330 Brookline Avenue (HIM 944), Boston, Massachusetts 02215, and Department of Pharmacology and Molecular Toxicology, University of Massachusetts, Medical School, 55 Lake Avenue North, Worcester, Massachusetts, 01655*

*Received July 31, 1996*⊗

ABSTRACT: The conformation of the three cyclic antagonist analogs of parathyroid hormone-related protein (PTHrP)-(7−34) {[Lys$^{13}$, Asp$^{17}$]PTHrP-(7−34)$NH_2$, [Lys$^{26}$, Asp$^{30}$]PTHrP-(7−34)$NH_2$, [Lys$^{13}$, Asp$^{17}$, Lys$^{26}$, Asp$^{30}$]PTHrP-(7−34)$NH_2$} is investigated by CD, NMR, and extensive computer simulations in aqueous solution and a TFE:water mixture. The structural analysis of these peptides, designed to stabilize different regions of the sequence in α-helical conformations, is an important step in addressing the correlation between helical content and binding affinity and bioactivity in this hormone−receptor system. Results from CD and NMR spectroscopy of all three analogues in aqueous solution indicate the presence of α-helix only in regions containing a 20-membered lactam ring. Upon addition of TFE, the three analogues display differences in the anticipated increase in helical content. The high-resolution structures produced at 50:50 TFE:water indicate specific differences in the extent and location of the helical regions. These conformations provide insight into the biological profiles of these analogues, reported in the previous manuscript [Bisello et al. (1997) *Biochemistry 36*, 3293−3299]. Since all three analogues are α-helical in the C-terminal region (residues 25−34 have been previously identified as containing the binding domain) and display similar binding affinities, we conclude that this conformational feature is important for the interaction between the peptide and the receptor. The extent of the helix (toward the N-terminus) and the presence of a hinge in the central region of the peptide play roles in the observed efficacy as measured by antagonism of PTH-stimulated adenylyl cyclase activity. The most active analogue consists of helical segments from residues 13−18 and 20−34, separated by a kink centered at Arg$^{19}$.

The predominant form of the recently discovered parathyroid hormone (PTH)-related protein (PTHrP)[1] contains 141 residues and is a secretory product of human tumors associated clinically with the syndrome of humoral hypercalcemia of malignancy (Suva et al., 1987). The role of PTHrP in normal physiology of adult animals has not been completely elucidated. The 1−34 N-terminal fragments of PTHrP and PTH, a major regulator of extracellular calcium homeostasis, are equipotent and retain all the calciotropic activity characteristic of the intact hormones (Horiuchi et al., 1987; Kemp et al., 1987; Yates et al., 1988). Both PTH and PTHrP interact with the same receptor which belongs to a unique subfamily of seven transmembrane domain-containing, G-protein coupled receptors. In spite of their functional similarity, PTH and PTHrP share very limited sequence homology which is mostly localized at the N-terminal domain; eight out of the 13 N-terminal amino acid residues are identical. Truncation of the first six N-terminal residues removes the principal "activation domain," yielding either PTH-(7−34), a weak antagonist (Horiuchi, et al., 1983), or PTHrP-(7−34), a partial agonist (McKee, et al., 1988), of the PTH/PTHrP receptor (Rosenblatt, 1986). The truncation of the first six N-terminal residues substantially reduces the sequence homology in the 7−34 fragments of PTH and PTHrP, eliminating four out of eight identical residues. These findings suggest that the comparable binding affinity of PTH-(7−34) and PTHrP-(7−34) is a result of similar bioactive conformations at the receptor binding site (Chorev et al., 1990).

According to a CD study, conducted in water at pH 4.5, PTHrP-(7−34)$NH_2$ was found to have no α-helix (Barden & Kemp, 1989). However, in the presence of anionic amphiphiles, this partial agonist contains 30% α-helical structure (Chorev et al., 1993). Previous conformational

† This work was supported, in part, by Grants RO1-DK47940 (to M.R.) and GM54082 (to D.F.M.) from the National Institutes of Health.

* To whom correspondence should be addressed. Phone: (508) 793-7220. FAX (508) 793-8861. E-mail: dmierke@clarku.edu.

‡ University of Padova.

§ Clark University.

|| Beth Israel Deconess Medical Center.

⊥ University of Massachusetts.

⊗ Abstract published in *Advance ACS Abstracts,* March 1, 1997.

[1] Abbreviations: CD, circular dichroism; COSY, correlation spectroscopy; DADD, distance and angle driven dynamics; DG, distance geometry; DMPG, dimyristoylphosphatidylglycerol; MD, molecular dynamics; NMR, nuclear magnetic resonance; NOESY, nuclear Overhauser enhancement spectroscopy; PTH, parathyroid hormone; PTHrP, parathyroid hormone-related protein; SDS, sodium dodecyl sulfate; TFE, trifluoroethanol; TOCSY, total-correlation spectroscopy.

S0006-2960(96)01903-4 CCC: $14.00 

studies of two highly potent, pure antagonists, [Nle$^{8,18}$,D-Trp$^{12}$,Tyr$^{34}$]PTH-(7−34)$NH_2$ and [Leu$^{11}$,D-Trp$^{12}$]PTHrP-(7−34)$NH_2$, derived from PTH and PTHrP, respectively, indicate the presence of a long α-helical stretch in (1:1 v/v) TFE:water solvent (Chorev et al., 1995). The helical domain spans residues 16−26 and 16−32 in the PTH and PTHrP antagonist, respectively, with the latter being more stable. In addition, *β*-turns were identified at Asp$^{10}$-Leu-D-Trp-Lys$^{13}$ and Leu$^{11}$-D-Trp-Lys-His$^{14}$ in the PTHrP and PTH analogue, respectively. Introduction of hydrophobic residues, as in [D-Trp$^{12}$]PTHrP-(7−34)$NH_2$ and [Leu$^{11}$, D-Trp$^{12}$]PTHrP-(7−34)$NH_2$, increase affinity and antagonist potency with no further increase in α-helix content (Chorev et al., 1993).

In an attempt to increase α-helix propensity we have introduced (*i*)−(*i*+4) side chain-to-side chain cyclization via lactam bridge formation, as in [Lys$^{13}$, Asp$^{17}$]PTHrP-(7−34)$NH_2$. This modification results in about a 16-fold increase in affinity and is associated with 45% helicity in the presence of SDS−DMPG (Chorev et al., 1993). To further explore the correlation between helix-forming propensity and bioactivity in the antagonist series, we have studied the following structurally constrained PTHrP analogues, containing (*i*)−(*i*+4) lactam-bridged side chains:

[Lys$^{13}$, Asp$^{17}$]PTHrP-(7−34)$NH_2$ (**I**)

[Lys$^{26}$, Asp$^{30}$]PTHrP-(7−34)$NH_2$ (**II**)

[Lys$^{13}$, Asp$^{17}$, Lys$^{26}$, Asp$^{30}$]PTHrP-(7−34)$NH_2$ (**III**)

As reported in the preceding article in this issue [Bisello et al. (1997)], all three analogues display moderate to good binding affinities to the PTH/PTHrP receptor. Functional antagonism of PTH-stimulated adenylyl cyclase activity was observed for analogues **I** and **III**. Analogue **II** displays a very unusual pharmacological profile. Despite binding with high affinity, only weak functional agonistic and antagonistic properties are observed. The constraints introduced via side chain-to-side chain cyclization were designed to stabilize the helical structure in different portions of the molecule (Houston et al., 1995). Assuming that the helical structure is a major feature of the bioconformation of PTHrP-derived antagonists, a salt bridge between the side chains of Lys$^{13}$ and Asp$^{17}$ could be invoked as a stabilizing factor for a hypothetical N-terminal helix in the native sequence (Marqusee & Baldwin, 1987; Sholtz et al., 1993). Lactamization of Lys$^{13}$ and Asp$^{17}$ side chains (analogues **I** and **III**) will replace the reversible salt bridge with a permanent covalent bond, thus enhancing the stability of the underlying α-helix.

The second lactam bridge connecting the side chains of residues in positions 26 and 30 (analogues **II** and **III**) was carried out to stabilize a previously demonstrated propensity for α-helix at the C-terminal domain. In this case native residues His$^{26}$ and Glu$^{30}$ were replaced by Lys and Asp, respectively. The choice of L-Lys(*i*) and L-Asp(*i*+4) for the lactamization was also suggested by the findings of Felix and co-workers (1988) as a modification which facilitated the intrinsic ability of a 20-member lactam ring to promote helix folding. The lactam bridges were synthesized both singularly (analogues **I** and **II**) and simultaneously (analogue **III**) to investigate their intrinsic properties and examine possible synergistic effects. In the present study we report the conformational analysis of these three analogues by CD and NMR in TFE:water mixtures. The resulting structures are refined by extensive distance geometry calculations.

## MATERIALS AND METHODS

*CD Spectroscopy*. Spectra were obtained on a JASCO J-600 spectropolarimeter at room temperature in the wavelength range between 185 and 255 nm, using quartz cells with optical pathlength of 0.001, 0.005, 0.01, and 0.1 cm. Typically six to ten spectra were averaged and then analyzed using the software provided by JASCO. The instrument was calibrated with ammonium D-camphorsulfonate as specified by the manufacturer. Concentrations of the peptides were obtained by amino acid analysis. Evaluations of helical content were based on the Greenfield and Fasman (1969) method.

*NMR Spectroscopy and Signal Assignments*. Samples of each peptide were dissolved in a 1:1 mixture of $H_2O$:TFE-$d_3$ (CIL, Cambridge, MA), concentration 3 mM, volume 0.5 mL. The samples were tested for aggregation by CD measurements at different peptide concentrations. 1D and 2D $^1$H NMR spectra were recorded on a Bruker AM 400 spectrometer without spinning at 298 K. Data processing was performed on a Bruker X-32 workstation. All 2D spectra were acquired using the time proportional phase incrementation method (Bodenhausen et al., 1980), collecting 320−640 experiments of 2K data points. Prior to Fourier transformation, the time domain data was multiplied by $\pi/2 - \pi/3$ shifted squared sine bell or Gaussian window functions in both dimensions and zero filled to 2K × 1K real points. Third-order polynomial baseline correction was performed in the $F_2$ dimension after transformation. DQF-COSY spectra (Rance et al., 1983) were acquired using appropriate phase cycling to suppress rapid pulse artifacts (Derome & Williamson, 1990). In CLEAN-TOCSY spectra (Bax & Davis, 1985; Griesinger et al., 1988), obtained with a MLEV-17 spin-locking sequence, the mixing time ranged between 65 and 75 ms, the trim pulses were 2.5 ms, and the spin-lock field strength was 6.2 KHz. NOESY spectra (Bodenhausen et al., 1984) were recorded using mixing times of 200 ms with a 10% random variation of the mixing period to reduce ZQ coherence contributions (Macura et al., 1980). Chemical shifts were calibrated by TMS as an internal standard. In all cases the standard strategy for protein structure elucidation by $^1$H NMR spectroscopy was used (Wüthrich, 1986).

*Structure Calculations*. The volumes of the integrated cross-peaks from the NOESY spectra were determined using the AURELIA software. The calibration in amide regions were based on sequential NH-NH cross-peaks (2.80 Å in the helical state). Aliphatic regions required a different calibration based on the cross-peak of two methylene *β* protons (1.78 Å). The resulting distances were then classified in four classes, with upper limits of 2.8, 3.2, 3.5, and 4.0 Å, respectively. In those cases where stereospecific assignment was not possible, the upper distances were further relaxed by means of pseudoatom corrections (Wüthrich et al., 1983), yielding two classes of 5.0 and 6.0 Å. The values thus obtained were used as upper limits in the distance geometry calculations, while the lower limit was 1.80 Å in all cases. The distance geometry calculations were carried out with a home-written program utilizing the random metrization algorithm of Havel (1991) and run on Silicon Graphics

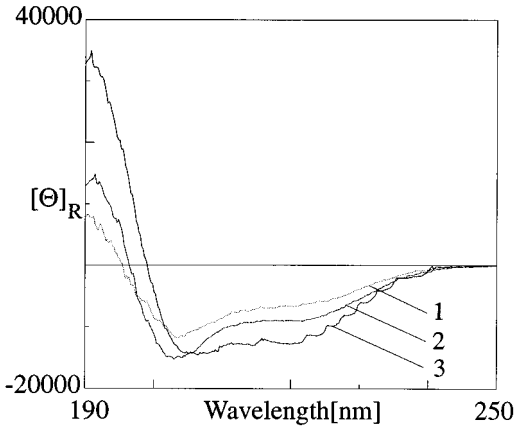


FIGURE 1: CD spectra of cyclic PTHrP lactam analogues **I** (13 $\mu$M, 5.4 pH), **II** (17 $\mu$M, 5.4 pH), and **III** (17 $\mu$M, 5.4 pH) in aqueous solution.

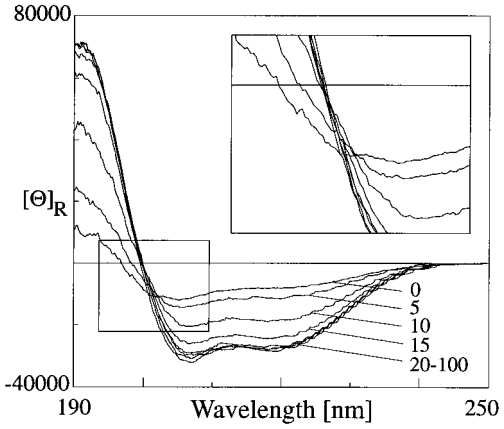


FIGURE 2: CD spectra of analogue **I**, concentration 15 $\mu$M, in water:TFE solution at various TFE concentrations (v/v indicated). The expansion illustrates the shift of the 208 nm absorption band observed for the 100% water solution.

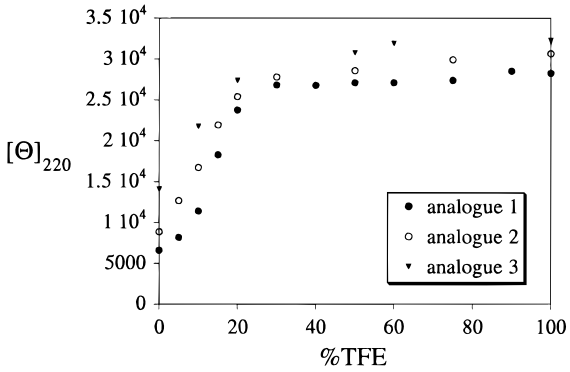


FIGURE 3: Onset of α-helix in analogues **I**-**III** on addition of TFE. Plots are of molar ellipticity at 220 nm as a function of TFE concentration in acidic aqueous solutions.

workstations. Experimentally determined distances, which were more restrictive than the geometric distance bounds (holonomic restraints) (Crippen & Havel, 1988), were added to create a distance matrix. The structures were first embedded in four dimensions and then partially minimized using conjugate gradients (Kaptein et al., 1988) followed by distance and angle driven dynamics (DADD) (Mierke et al., 1994). The DADD simulation was carried out at 500 K for 100 ps and then the temperature was gradually reduced over the next 40 ps. The DADD procedure utilizes the holonomic and experimental distance restraints plus a chiral penalty function for the generation of the violation "energy" and forces. The resulting structures were then reduced to three-dimensions using metrization and the optimization and DADD procedure repeated. Energy minimization and interactive modeling were performed using Discover (Consistent Valence Force Field, CVFF91) and Insight II (Biosym Technologies Inc., San Diego, CA). Analyses of the structures in terms of NOEs violations, order parameter values and dihedral angle distribution were performed using home-written programs.

## RESULTS

*CD Measurements*. The CD spectra of the three peptides in aqueous solution at pH ∼4 are shown in Figure 1. The spectra are concentration-independent in the range of $10^{-5}$−$10^{-3}$ M, and also pH-independent in the range of 3.5−7.0 (data not shown). Analogues **I** and **II** exhibit CD spectra with a similar shape, and estimated helix contents of ∼18% and ∼25%, respectively, corresponding to five and seven helical residues. Under similar conditions, linear PTHrP(7−34) is practically in the random coil conformation. Thus the lactam cyclizations increase the helix content of the PTHrP peptide, particularly when the bridge is at the C-terminus. The double-bridged analogue **III** reaches almost 40% helical content and the shape of the CD spectrum, in contrast to those observed for analogues **I** and **II**, is the classical one of a mixture of α-helix and random coil. The different shapes of the CD spectra of analogues **I** and **II** suggest contributions from structural elements different from α-helix.

Upon addition of TFE, there is an increase of the helix content for all three analogues (Figure 2). However, the spectra recorded in water of analogues **I** and **II** do not fit precisely the same isodichroic point of the spectra recorded in the presence of TFE. This is also an indication that in analogues **I** and **II** in water there is a contribution to the optical activity from structures different from an α-helix. This could be the reason for the different TFE-induced folding pathway of the three analogues, revealed by the profiles of the plots of molar ellipticity at 220 nm versus TFE content (Figure 3). In the case of analogue **I,** an S-shaped profile is observed, while analogue **II** and the double-bridged analogue **III** exhibit exponential profiles.

In all cases, saturation conditions, in terms of maximum helix content, are reached at ∼30% TFE. The maximum helix content ranges from 75% for analogue **I** to ∼90% for analogue **III** with two lactam bridges. These figures are consistently higher than that reported for linear PTHrP-(7−34) (Cohen et al., 1993) and confirm the enhanced helix-forming propensity of the constrained analogues in this solvent medium.

*NMR Measurements*. To gain further detail on the conformations of these constrained analogues, NMR experiments were carried out in 1:1 (v/v) $H_2O$-TFE-$d_3$, conditions in which the peptides are at the maximum of helix content according to the CD results. The proton resonance assignment of the three peptides was achieved by standard procedures: spin systems were assigned using DQF-COSY and TOCSY spectra; sequence-specific assignments were achieved through NOESY experiments. Proton resonances are reported in Tables I−III of Supporting Information. As an example, the amide region of the NOESY spectra of the peptides **I**−**III** are reported in Figure 4. The number and the intensity of NH($i$)-NH($i$+1) and NH($i$)-NH($i$+2) cross-peaks are a clear indication of highly helical peptides. In

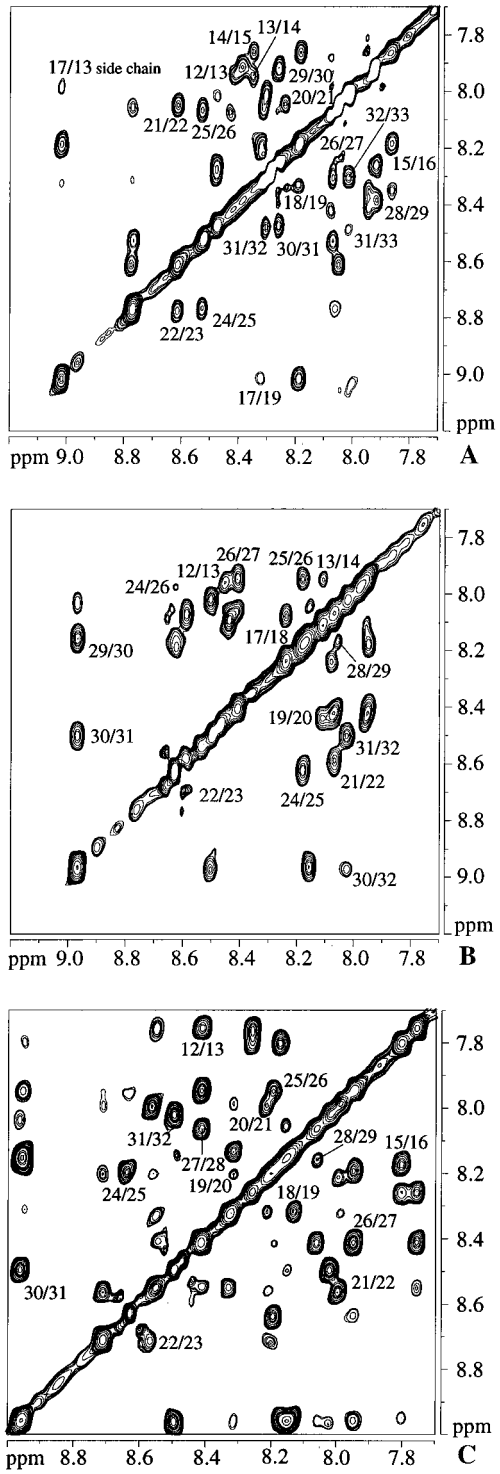


FIGURE 4: Amide region of NOESY spectra in 1:1 $H_2O$:TFE-$d_3$: analogue **I** (A), analogue **II** (B), and analogue **III** (C) (concentration, 3 mM; mixing time, 200 ms; temperature, 300 K; pH 3.5−5.0). Some of the sequential connectivities are indicated.

Figure 5, the summary of NOESY connectivities relevant for the assessment of secondary structure is reported. From the NOE pattern [αH(*i*)-NH(*i*+3) αH(*i*)-*β*H(*i*+3), Figure 5A] of analogue **1,** it is possible to identify a long helical segment from residue Lys[13] to Ala[34], although the region Asp[17]-Arg[19] is affected by severe resonance overlap. Nevertheless, the two groups of signals are joined together by a strong NH(18)-NH(19) and a NH(17)-NH(19) cross-peak. Sequential αH-NH signals of medium-to-weak intensity are present all along the sequence; while two groups of αH(*i*)-NH(*i*+4) signals are observed for positions 13−18 and 22−32. The highly negative values (<−0.18) of the secondary shifts of the Cα protons (Figure 6A) from residue Lys[13] to His[32], corroborate these conclusions. The segment 13 to 34 corresponds to ∼80% of the entire sequence, thus the extent of α-helical content in analogue **I** found by NMR appear to be in good agreement with the amount of helix estimated from the CD spectra. Thus, with respect to previously published results on PTHrP-(7−34) (Chorev et al., 1995), the lactam bridge effectively contributes to the stabilization of the helical structure in the N-terminal portion of the molecule. NMR spectra of this analogue in water were also collected and examined. The presence of NH(*i*)-NH(*i*+1) NOEs for residues 12−19 and αH(14)-NH(17), αH(15)-NH(18) pointed out that the loop formed by the bridge was the only contribution to helix structure in water solution.

The NOE pattern of analogue **II** shows medium-range connectivities, (*i*)-(*i*+3) and (*i*)-(*i*+4), from residue Lys[13] to residue Ala[34], corresponding to ∼80% helix as for analogue **I**. However, the NOEs at the N-terminus are weaker in this case (Figure 5B) and also the secondary shifts of the Cα protons are smaller toward the N-terminus (Figure 6B), indicating significant flexibility in this part of the molecule as compared to **I**. This confirms that the lactam bridge at the N-terminus stabilizes the helical structure while the C-terminal lactam bridge does not further enhance an already present high tendency toward the helical arrangement. The presence of a medium NOE cross-peak NH(27)-αH(28) in the middle of the bridged region is noteworthy. This finding does not agree with the typical helix structure, and could be a feature of this particular bridge itself, since the corresponding peak was not present in analogue **I**.

The NOESY spectra of the double-bridged analogue **III** contain the largest number of cross-peaks, but fortunately they are the least affected by signal overlap (Figure 4C). Again, in this case, the sequence 13−34 is clearly helical, as shown by the NOE pattern (Figure 5C) and the secondary shifts of the Cα protons (Figure 6C). The presence of cross-peaks like NH(11)-NH(13) and αH(11)-NH(14) is a clear indication of a helix stretch spanning further toward the N-terminus when compared to peptides **I** and **II** which contain single lactam bridges. NOE cross-peaks NH(*i*)-αH(*i*+1), not consistent with an α-helix, are observed in the middle of both lactam-bridge regions, NH(14)-αH(15) and NH(27)-αH(28). NMR spectra of this analogue in 1:1 $D_2O$/TFE-$d_3$ solution give a clear indication of the presence of hydrogen bonds. NH signals of residues Gln[16] to Ile[31] are all present 24 h after sample preparation. After 10 days, the NH of residues Leu[18] and Lys[26]-Asp[30] are still observable.

*Distance Geometry Calculations.* Integration of the NOESY spectrum of analogue **I** provided 256 constraints, 228 of which were conformationally informative (115 intraresidue and 113 interresidue). The DG calculations produced 80 structures which had 40 violations of the distance constraints, the largest of which was 1.0 Å, an indication of agreement between calculated structures and experimental NMR data. The backbone dihedral angle order parameters (Havel, 1990) were calculated for the structures (Figure 7A). This plot exhibits an ordered structure (order parameter < 0.7) for the segment comprising residues 13−34 with the exception of Leu[18] and Arg[19]. The backbone dihedral angles of Lys[13] to Asp[17] lie in the helix region of the Ramachandran map. Low-order parameter values for

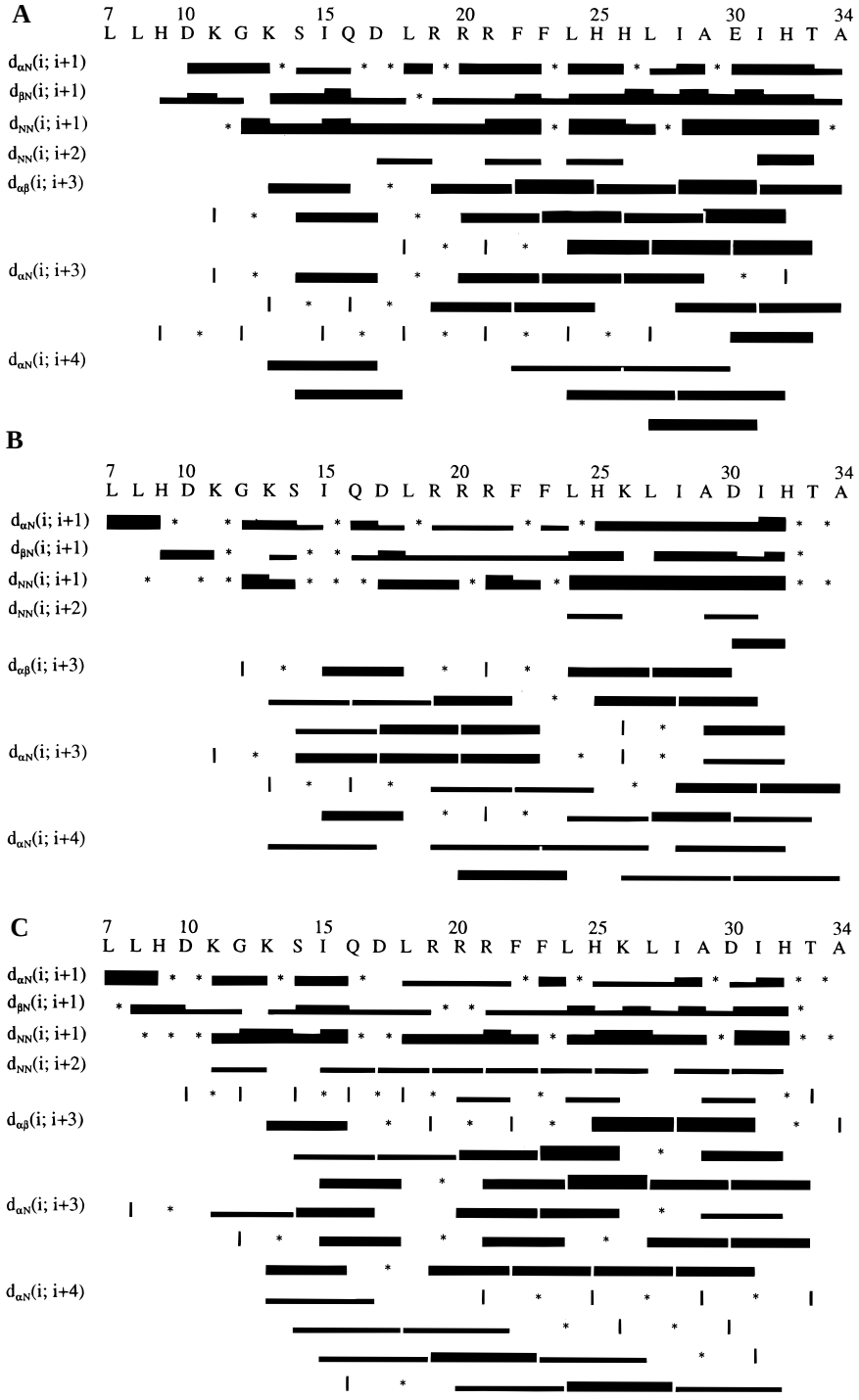


FIGURE 5: Summary of observed NOEs for analogue **I** (A), analogue **II** (B), and analogue **III** (C), in 1:1 $H_2O$:TFE-$d_3$. Peaks are grouped into three classes on the basis of their integrated volumes. Asterisks indicate the likely presence of a peak which could not be confirmed because of signal overlap.

residue Leu[18] is the result of two possible conformations: ($\phi$ 60°, $\psi$ 20°) and ($\phi$ −60°, $\psi$ 20°); the latter is the most populated and responsible for a turn in the structure. Arg[19] $\phi$ appears spread over values ranging from −120° to +60°, mostly centered around -60°. Therefore the discontinuity in the middle of the peptide chain can be attributed solely to Arg[19] $\phi$. All of the residues following this point, Arg[20] to Ala[34], display backbone dihedral angles typical of helical secondary structure. The best structure in terms of violation of the penalty function was energy minimized using conjugated gradients, and the result is shown in Figure 8A. The global picture consists of two well-defined helical segments, 13−18 and 19−34, separated by a 90° kink. There is no tendency of Gly[12] to fold into the N-terminus helix; this residue prefers an extended conformation.

Distance geometry calculations on analogue **II** were carried out using 280 distance constraints, 226 conformationally informative (119 intra-residue and 107 inter-residue) resulting in 82 structures. The largest violation to the experimental distances was 1.5 Å out of a total of 20. In Figure 7B the order parameter values of backbone dihedral angles are given. Well defined structure is observed only in the C-terminus, after Ile[15]. Conversely, no disruption of convergence is detected all along the segment 15−34. The inspection of the Ramachandran map of residue Ser[14] and Ile[15] indicates the presence of a turn resembling a type II $\beta$-turn; in fact the major conformational family for these two residues have backbone dihedral values of (-90°, 150°) and

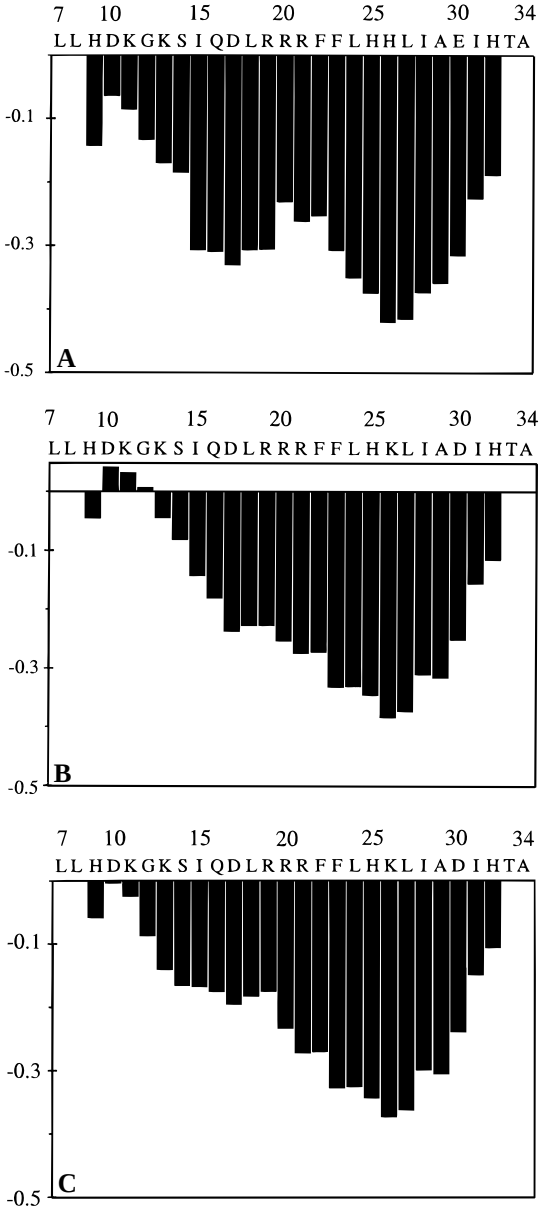


FIGURE 6: Chemical shift differences of the Cα protons of analogue **I** (A), analogue **II** (B), and analogue **III** (C), in 1:1 $H_2O$:TFE-$d_3$. The values shown have been averaged with the chemical shift differences of the adjacent residues.

(60°, 0°), respectively. The remaining residues, 16−34, are located in the helix region with the exception of the amino acids around position 24, in which a deviation of the $\psi$ dihedral angles toward positive values was detected. This trend results in a conformation of the peptide with a slight bend in the helical stretch (Figure 8B). The bend is principally a result of the conformation of residues Phe[23] and Lys[26], with $\phi$ and $\psi$ values of (-80°, 0°) and (-90°, 30°), respectively, that subsequently project their carbonyl groups out of the helical axis. This distortion of the α-helix does not seem to be caused by the unusual, non-helical NOE, NH(27)-αH(28), since similar NOEs were observed for both lactam bridges for analogue **III** and yet the resulting conformation (discussed below) displays no helical distortion in the region of the lactams.

Structure calculations of the double-bridged analogue **III** made use of 327 experimental NOEs, 279 of which were informative (135 were intra-residue constraints and 144 inter-residues) and resulted in 82 structures. There were 26 distance constraint violations with 1.0 Å as the largest

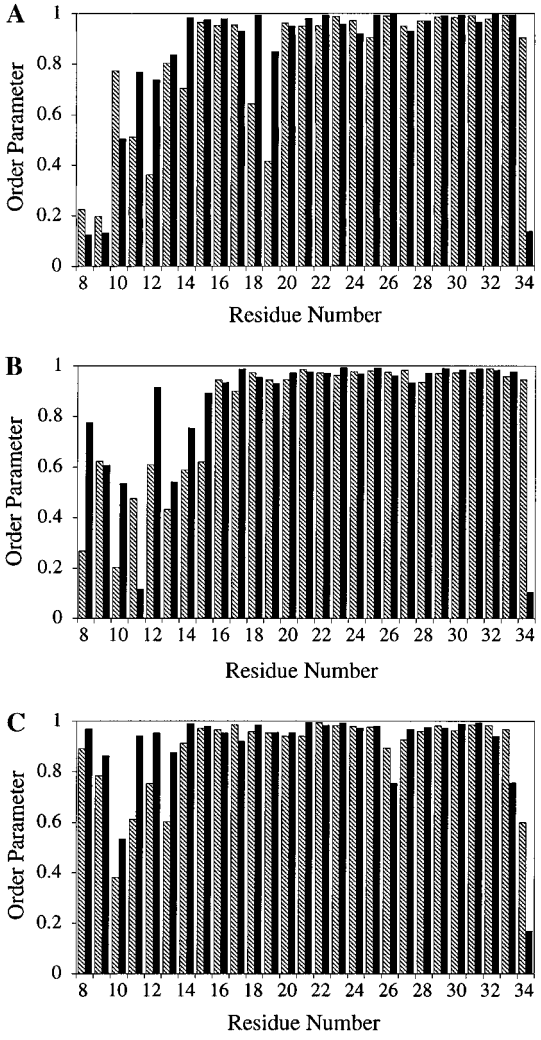


FIGURE 7: Order parameter values of the backbone dihedral angles calculated for the ensemble of structures obtained from the distance geometry calculations: analogue **I** (A), analogue **II** (B), and analogue **III** (C).

violation. The result of the order parameter analysis on backbone dihedrals is shown in Figure 7C. This analogue displays the largest extent of defined structure, beyond the expected well ordered α-helix, residues 13−34. In addition, Lys[11] and Gly[12] show a tendency to fold into a definite structure, presenting backbone dihedral angle values of 60°, 30° and −90°, −30°, respectively. The global shape is a long helix-like segment, although a number of residues deviate from standard dihedral angles for an α-helix. The most populated family of Lys[13] has $\phi$ and $\psi$ values of −120°, 60°, while residues Arg[19], Phe[22], Phe[23], and Ile[28] display $\psi$ values removed from typical helix values. The Ramachandran plot for Lys[26] shows two possible conformations, (−120°, 30°) and (−60°, −50°), with the helix region the most populated. The results from energy minimization of the structure with the smallest penalty function is shown in Figure 8C. A helix-like conformation starts from residue Asp[10], while Lys[13] (−160°, 70°) introduces a distortion and its carbonyl group is out of the helical axis. The well-folded helix stretch spans from residue Ser[14] to the end of the molecule, disrupted by a turn around residue Arg[19] (−100°, 40°). The presence of a continuous helix stretch spanning from at least residue Gly[12] to residue Ile[31] is further supported by the results of deuterium exchange rates of the amide protons in analogue **III**.

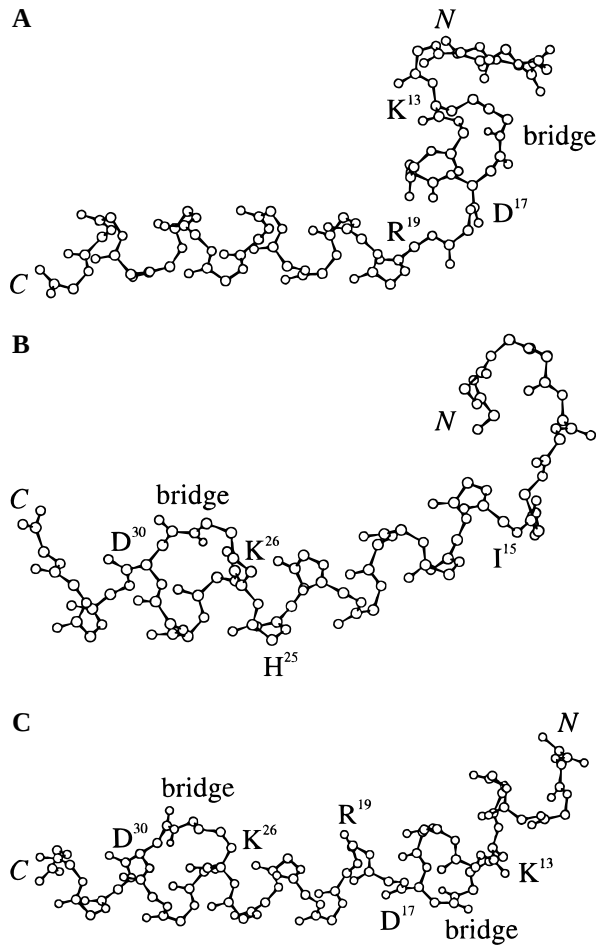


FIGURE 8: Ball-and-stick depiction of analogue **I** (A), analogue **II** (B), and analogue **III** (C), of the DG-generated structure with the lowest penalty function after energy minimization.

Unfortunately, no detailed information of the lactam bridge chain conformation was obtained for the peptides. This is a consequence of the lack of NOEs between the side chains and the backbone mainly due to overlapping signals in the aliphatic region. Therefore, experimental data does not allow for the determination of the relative orientation of the peptide bond in the lactam with respect to the helix direction.

## DISCUSSION

CD and NMR investigations confirmed that the antagonist containing a monocyclic N-terminal lactam (analogue **I**) adopts in aqueous solution a helix conformation confined to the loop region connected by the lactam bridge, approximately five residues in length. In the same solvent, the antagonist containing a monocyclic C-terminal lactam (analogue **II**) presents a higher content of helix, with a 7-residue long stretch estimated from the CD spectrum. The CD spectrum of the double-bridged analogue **III** in water solution is more intense than those of analogues **I** and **II**; however, the estimation of 11 residues involved in a helix suggests no synergistic effects of the two bridges on stabilizing the α-helical motif. The band from the $\pi-\pi^*$ transition (often called the 208 nm absorption band) is observed at ∼202 nm for both of the monocyclic analogues (**I** and **II**); this pronounced shift of the absorption band is the result of the presence of a distinct conformation, different from helix (Figure 1). This second conformation was not observed by NMR spectroscopy; the NOESY spectra of analogue **I** in water indicates defined secondary structure only in the region of the lactam bridge (the NOEs are consistent with an α-helix). The CD spectrum of the double lactam-containing analogue (**III**) displays no such shift of the "208 nm" absorption band and therefore is similar to the classical, two-state, random-coil/helix CD spectrum.

Upon addition of TFE, the helix content increases as anticipated. In analogues containing a lactam bridge at the C-terminus (analogues **II** and **III**), the folding process follows an exponential curve (Figure 3), which suggests the continuous extension of the C-terminal helix by adjacent residues upon the increase in the concentration of TFE. In contrast, analogue **I** showed a sigmoid folding curve, indicating the absence of a continuous propagation of the helical content upon the addition of TFE (the folding follows two-step kinetics). Therefore, when the lactam is in the midregion of the peptide (analogue **I**), a significant increase in the hydrophobicity of the medium is required before further propagation of the folding process will take place. Thus, despite the tendency of the C-terminus to adopt an α-helix, even in linear PTHrP-derived peptides, the N-terminal helix of analogue **I** does not propagate steadily toward the C-terminus upon the addition of TFE; there is a cooperative induction of the helical structure once sufficient TFE has been introduced (∼10% TFE) (Figure 3).

In 1:1 $H_2O$:TFE, the solvent conditions used for the NMR investigations, all the analogues reach the highest folded conformation, with the bicyclic analogue **III** showing the largest helix extent derived from a well-defined stretch including residues 13−34 and a helix-like conformation in the N-terminal region preceding $Lys^{13}$. The helix content of the monocyclic analogues **I** and **II** as determined by NMR are quite similar, although the midregion bridged compound (analogue **I**) contains a two-residue longer helical stretch. This slight difference is consistent with the NOEs, in that the medium-range NOEs (*i*)-(*i*+3) and (*i*)-(*i*+4), observed for analogue **II** are weaker in intensity and therefore consistent with greater conformational flexibility. The fact that the CD spectra of the monocyclic analogues **I** and **II** predict identical helical contents can be explained by taking the helix macro-dipole effect into account. Under the assumption that $Leu^{18}$ is involved in a turn-like conformation concomitant with the lack of conformational information on $Arg^{19}$ ($\phi$), we may suggest the presence of two separate helix stretches in analog **II**. The anticipated CD spectra of two consecutive, non-continuous helices would be less intense than the spectra of a uniformly continuous helix stretch containing the same number of residues.

The biological activities of these peptides (Bisello et al., 1997, preceding article; Chorev et al., 1991), are dependent on their capacity to bind to the PTH/PTHrP G-protein-coupled receptor. Previous studies have demonstrated that the principal binding domain consists of residues 25−34 (Rosenblatt, 1986) of the N-truncated peptide (Caulfield et al., 1990). This is further substantiated by the present studies; all three analogues display a well-defined α-helix in the C-terminus and all three display similar binding affinities (18, 23, and 100 nM for analogues **I**, **II**, and **III**, respectively). These binding affinities are comparable to the affinity ($k_b$ = 28 nM) measured for [$Leu^{11}$,D-$Trp^{12}$]PTHrP-(7−34)$NH_2$, one of the most potent PTH antagonists synthesized to date (Nutt et al., 1990). Thus, the close association between binding to the PTH/PTHrP receptor and the stabilization of the helix-like motif at the C-terminus via *i*,*i*+4 side chain-to-side chain lactam cyclization is fully

consistent with an α-helix as an integral part of the antagonist-relevant bioactive conformation.

The moderate reduction in binding affinity and potency (for inhibiting PTH-stimulated adenylyl cylase) of analogue **III** compared to the activity profile observed for analogue **I** suggests a functional role for the bend motif about residues $Asp^{17}$-Leu-Arg-$Arg^{20}$ found in **I**. The absence of this hinge region in the bicyclic lactam **III** may interfere with its capacity to attain an optimal interaction with the PTH/PTHrP receptor.

The discrepancy between the good binding affinity and very poor potency (either as an agonist or as an antagonist) of the monocyclic, C-terminal-containing lactam analogue **II** is more difficult to reconcile, both pharmacologically and structurally. The increased flexibility at the N-terminus of moncyclic lactam **II** as compared to analogues **I** and **III** may produce this "non-classical" pharmacological profile. In both functionally active antagonists, analogues **I** and **III**, both of which contain a lactam ring between $Lys^{13}$ and $Asp^{17}$, the N-terminus is more constrained and therefore more structured. The difference between the location of the bend in analogues **I** (centered around $Arg^{19}$) and **II** (centered around $Ile^{15}$) also may produce the lack of functional activity observed for analogue **II**. The relationship between structural motifs revealed in this study and the dissociation between binding affinity and functional potency observed for [$Lys^{26}$,$Asp^{30}$]PTHrP-(7−34)$NH_2$ (**II**) is unique; the mechanism awaits elucidation. Interestingly, the same monocyclization at the C-terminal portion of the PTHrP-(1−34) results in a larger decrease in affinity than in agonist potency as compared to the equipotent midregion monocyclic and bicyclic lactam agonists (Bisello et al., 1997, preceding manuscript).

In conclusion, the present conformational studies of the three lactam ring-containing PTHrP-(7−34) sequences in TFE:water, attributes different conformations to each analogue reflecting the number and location of the lactam rings. To further understand the relevance of these conformations to the different biological profiles will require the validation of these structures under different conditions (e.g., in the presence of a membrane mimetic) and a more expansive set of analogues specifically modified at the location of interest (e.g., hinge region). These investigations are currently underway in our laboratories.

## SUPPORTING INFORMATION AVAILABLE

Proton chemical shifts of the three analogues (Tables I−III) and CD spectra of analogues **II** and **III** in water:TFE at various TFE concentrations (5 pages). Ordering information is given on any current masthead page.

## REFERENCES


Barden, J. A., & Kemp, B. E. (1989) *Eur. J. Biochem. 184*, 379−394.

Bax, A., & Davis, D. G. (1985) *J. Magn. Reson. 65*, 355−360.

Bisello, A., Nakamoton, C., Rosenblatt, M., & Chorev, M. (1997) *Biochemistry 36*, 3293−3299.

Bodenhausen, G., Vold, R. L., & Vold, R. R. (1980) *J. Magn. Reson. 37*, 93−106.

Bodenhausen, G., Kogler, H., & Ernst, R. R. (1984) *J. Magn. Reson. 58*, 370−388.

Caulfield, M. P., McKee, R. L., Goldman, M. E., Duong, L. T., Fisher, J. E., Gay, C. T., DeHaven, P. A., Levy, J. J., Roubini, E., Nutt, R. F., Chorev, M., & Rosenblatt, M. (1990) *Endocrinology 127*, 83−87.

Choen, F. E., Strewler, G. J., Bradley, M. S., Cariquist, M., Nilsson, M., Ericsson, M., Ciardelli, T. L., & Nissenson, R. A. (1991) *J. Biol. Chem. 266*, 1997−2004.

Chorev, M., Roubini, E., McKee, R. L., Gibbons, S. W., Goldman, M. E., Caulfield, M. P., & Rosenblatt, M. (1991) *Biochemistry 30*, 5968−5974.

Chorev, M., Goldman, M. E., McKee, R. L., Roubini, E., Levy, J. J., Gay, C. T., Reagan, J. E., Fisher, J. E., Caporale, L. H., Golub, E. E., Caulfield, M. P., Nutt, R. F., & Rosenblatt, M. (1990) *Biochemistry 29*, 1580−1586.

Chorev, M., Epand, R. F., Rosenblatt, M., Caulfield, M. P., & Epand, R. M. (1993) *Int. J. Pept. Protein Res. 42*, 342−345.

Chorev, M., Behar, V., Yang, Q. M., Rosenblatt, M., Mammi, S., Maretto, S., Pellegrini, M., & Peggion, E. (1995) *Biopolymers 36*, 485−495.

Crippen, G. M., & Havel, T. F. (1988) *Distance Geometry and Molecular Conformation*, John Wiley, New York.

Derome, A. E., & Williamson, M. P. (1990) *J. Magn. Reson. 88*, 177−185.

Felix, A. M., Heimer, E. P., Wang, C. T., Lambros, T. J., Fournier, A., Mowles, T. F., Maines, S., Campbell, R. M., Wegrzynsky, B. B., Toome, V., Fry, D., & Madison V. S. (1988) *Int. J. Pept. Protein Res. 32*, 441−454.

Greenfield, N., & Fasman, G. D. (1969) *Biochemistry 8*, 4108−4116.

Griesinger, C., Otting, G., Wüthrich, K., & Ernst, R. R. (1988) *J. Am. Chem. Soc. 110*, 7870−7872.

Havel, T. F. (1990) *Biopolymers 29*, 1565−1585.

Havel, T. F. (1991) *Prog. Biophys. Mol. Biol. 56*, 43−78.

Horiuchi, N., Holick, M. F., Potts J. T., Jr., & Rosenblatt, M. (1983) *Science 220*, 1053−1056.

Horiuchi, N., Caulfield, M. P., Fisher, J. E., Goldman, M. E., McKee, R. L., Reagan, J. E., Levy, J. J, Nutt, R. E., Rodan, S. B., Schofield, T. L., Clemens, T. L., & Rosenblatt, M. (1987) *Science 238*, 1566−1569.

Houston, M. E., Jr., Gannon, C. L., Kay, C. M., & Hodges, R. S. (1995) *J. Peptide Sci. 1*, 274−281.

Kaptein, R., Boelens, R., Scheek, R. M., & van Gunsteren, W. F. (1988) *Biochemistry 27*, 5389−5395.

Kemp, B. E., Moseley, J. M., Rodda, C. P., Ebeling, P. R., Wettenhall, R. E. H., Stapleton, D., Diefenbach-Jagger, H., Ure, F., Michelangeli, V. P., Simmons, H. A., Raisz, L. G., & Martin, T. J. (1987) *Science 238*, 1568−1570.

Macura, S., Huang, Y., Suter, D., & Ernst, R. R. (1980) *J. Magn. Reson. 43*, 259−281.

Marqusee, S., & Baldwin, R. L. (1987) *Proc. Natl. Acad. Sci. U.S.A., 84*, 8898−8902.

McKee, R. L., Goldman, M. E., Caulfield, M. P., DeHaven, P. A., Levy, J. J., Nutt, R. F., & Rosenblatt, M. (1988) *Endocrinology 122*, 3008−3010.

McKee, R. L., Caulfield, M. P., & Rosenblatt, M. (1990) *Endocrinology 127*, 76−82.

Mierke, D. F., Geyer, A., & Kessler, H. (1994) *Int. J. Pept. Protein Res. 44*, 325−331.

Nutt, R. F., Caulfield, M. P., Levy, J. J., Gibbons, S. W., Rosenblatt, M., & McKee, R. L. (1990) *Endocrinology 127*, 491−493.

Rance, M., Sørensen, O. W., Bodenhausen, G., Wagner, G., Ernst, R. R., & Wüthrich, K. (1983) *Biochem. Biophys. Res. Commun. 117*, 479−485.

Rosenblatt, M. (1986) *N. E. J. Med. 315*, 1004−1013.

Sholtz J. M., Qtan H., Robbins V. H., & Baldwin R. L. (1993) *Biochemistry 32*, 9668−9676.

Suva, L. J., Winslow, G. A, Wettenhall, R. E., Hammonds, R. G., Moseley, J. M., Diefenbach-Jagger, H., Rodda, C. P., Kemp, B. E., Rodriguez, H., Chen, E. Y., Hudson, P.J., Martin, T. J., & Wood, W. I. (1987) *Science 237*, 893−897.

Wüthrich, K. (1986) *NMR of Proteins and Nucleic Acids*, John Wiley, New York.

Wüthrich, K., Billeter, M., & Braun, W. (1983) *J. Mol. Biol. 169*, 949−961.

Yates, A. J. P., Gutierrez, G. E., Smolens, P. Travis, P. S., Katz, M. S., Aufdemorte, T. B., Boyces, B. F., Hymer, T. K., Poser, J. W., & Mundy, G. R. (1988) *J. Clin. Invest. 81*, 932−939.


BI9619031